Journal of Science and Technology – Engineering and Technology for Sustainable Development
Volume 36, Issue 2, April 2026 , 079–086

Sub-Synchronous Resonance Analysis for Wind Farm Utilizing Double-Fed Induction Generators Linked to Series Compensation Transmission System

Truong Ngoc Minh*
Hanoi University of Science and Technology, Ha Noi, Vietnam
**Corresponding author email: minh.truongngoc@hust.edu.vn*

Abstract

The integration of wind energy into electrical grid necessitated the incorporation of wind farms with series compensated transmission systems to guarantee power distribution. This article examines the occurrence of sub-synchronous resonance in wind farm utilizing double-fed induction generator. The system under examination is predicated upon a modified version of the IEEE Second Benchmark (SBM) model specifically designed for sub-synchronous resonance investigations. A dynamic model for the system has been proposed to facilitate an analysis of sub-synchronous resonance phenomena. Eigenvalue analysis is conducted in conjunction with simulation at various wind velocities and series compensation. The distinct oscillatory modes, including sub-synchronous resonance, supersynchronous resonance are subjected to comprehensive analysis. Simulation results are executed to substantiate the efficacy of the proposed methodology.

Keywords: Double-fed induction generator (DFIG), eigenvalue analysis, sub-synchronous resonance (SSR).

1. Introduction

Nowadays, with advancements in technology and increasing investments, wind energy has emerged as the most rapidly expanding sources of current electrical power systems.

Recognizing that wind energy installations are frequently sited at considerable distances from consumption areas, the requirement for high capacity and long transmission lines is critical for the efficient application of wind farm. To address the augmented output from wind energy sources, two alternatives are present: either the construction of new transmission infrastructures or the enhancement of existing lines to improve their power transfer. The establishment of new transmission lines is not a financially viable solution. Series compensation represents a proficient method for augmenting the transfer capacity of transmission lines. Consequently, series compensated transmission lines serve as an effective method for the integration of substantial wind generation into the electrical grid [1].

Considering that the series-compensated transmission lines can markedly enhance both the transmission capability and the stability margins of the electrical system. However, a possible risk of sub-synchronous resonance (SSR) is available. SSR emerges from the dynamics between wind energy conversion systems and transmission lines that are series-compensated, which could lead to the failure of the turbine-generator shaft and potential instability in power systems.

Multiple occurrences of SSR incidents have been reported. Wind farms utilizing double-fed induction generators (DFIG) were interconnected with a series compensation system, leading to numerous wind turbines experiencing tripping and damage to their circuits. In 2012, a series of SSR events were recorded, attributed to DFIG wind farms and their associated compensated lines, leading to a substantial disconnection of wind turbines [2].

Many reports have studied the potential hazards associated with SSR within wind energy installations. Frequency domain techniques [3], eigenvalue assessments [4], or an integration of both approaches have been suggested [5]. Utilizing frequency domain techniques significantly simplifies system modeling; however, it poses challenges in deriving comprehensive quantitative component involvement, oscillation amplitude, and so forth.

Eigenvalue analysis is more diagnostic and design-friendly than time-domain runs or simple spectral methods. This method offers significant insights into the possible oscillatory modes present at a specified operating condition. Hence, eigenvalue analysis is preferred because it directly finds unstable/sub-synchronous modes, quantifies frequency and damping, and links modes to physical components. The computed eigenvalues are indicative of the system's oscillation modes. Accurately determining the corresponding eigenvectors facilitates the identification of the predominant state variables, along with those that contribute minimally.

p-ISSN 3093-3242
e-ISSN 3093-3579
https://doi.org/10.51316/jst.189.etsd.2026.36.2.10
Received: Apr 13, 2025; Revised: Aug 27, 2025;
Accepted: Oct 2, 2025; Online: Mar 24, 2026

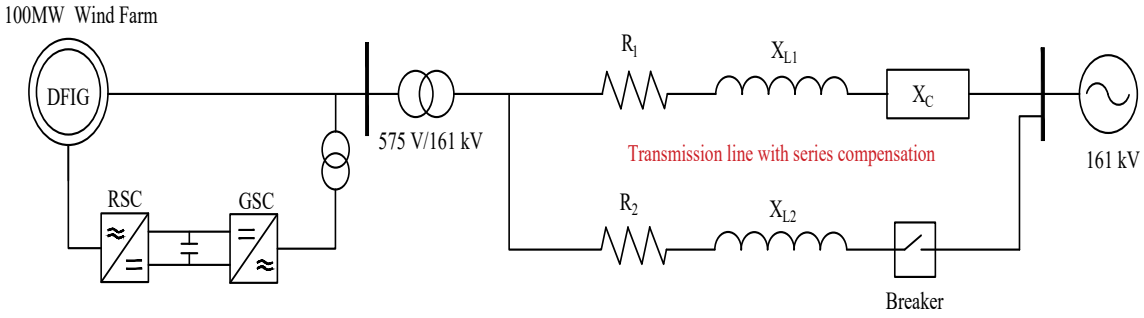

Fig. 1. The studied system utilizing DFIG

Therefore, this paper investigates the representation of wind farms utilizing DFIG that are linked to a series-compensated transmission system, and a precise analysis of SSR employing the eigenvalue approach.

Eigenvalue analysis for conventional turbine–generator system is well documented; however, enough literature is not available on SSR phenomenon in the context of series compensated wind farm systems. This analytical approach necessitates that the mechanical and electrical systems are represented by a linear framework of differential equations. Since a wind turbine-generator exhibits multiple sub-synchronous modes, the application of low order model is typically inadequate [6]. We proposed a detailed two-mass shaft mechanical and sixth-order generator model to derive full state matrix combining mechanical shaft, generator, and transmission line.

Moreover, eigenvalue-based SSR analysis depends on a correct linearization point; non-convergent or inaccurate initial state values lead to eigenvalues inconsistent with time-domain behavior. A method to compute initial states that improves convergence and eigenvalue accuracy aligning with time-domain simulations (MATLAB implementation) across wind speeds and compensation levels is also introduced.

This paper presents a methodology for modeling DFIG wind turbines connected to series-compensated transmission line available for SSR analysis. We start by developing a detailed model that includes mechanical and electrical system components. Using this model, the system is linearized, and eigenvalues are computed with respect to parameters (series compensation, wind velocity).

The rest of this paper is organized into the following sections. Section 2 presents the system with wind farm utilizing DFIG. Section 3 outlines the modeling of DFIG. In Section 4, the procedures of calculating system state for eigenvalue analysis is presented. In Section 5, simulation results obtained through linear model in MATLAB to find the dynamic characteristics of the system are presented. Finally, Section 6 concludes this paper.

2. The Studied Power System

A power system under examination involves a wind farm with a capacity of 100 MW, linked to an infinite bus via a 161 kV transmission line. The system is based on the Single-Machine Model (SBM), which has been extensively employed in SSR analysis. The configuration consists of two parallel transmission lines, one of which incorporates series compensation through the utilization of capacitor banks. The wind farm will become radially connected to a series-compensated transmission line when the circuit breaker on the non-compensated line is disengaged.

The schematic representation of the system is illustrated in Fig. 1. The parameters relevant to the studied system are presented in Table 1.

Table 1. System data

Transformer turn ratio	575 V/161 kV
Base apparent power	100 MVA
R_L	0.02 p.u.
X_L	0.5 p.u.
$X_{Transformer}$	0.14 p.u.
X_{system}	0.06 p.u.

The wind energy comprises 67 turbines, each possessing a nominal capacity of 1.5 MW, culminating in a total output of 100 MW [7]. This design employs a wound rotor induction generator (WRIG).

As illustrated in Fig. 1, the stator of generator is directly linked to the transmission system. The rotor of the generator interfaces with the grid via a converter. Since power is supplied to the grid from the stator and the rotor, this generator configuration is classified as DFIG. The converter regulates both the rotor frequency and rotor speed. Additionally, it facilitates reactive power compensation. The operational speed fluctuation is ±30% typically around the synchronous speed. A notable benefit of this system is the ability to harness lost power through an external variable resistance. Nevertheless, the principal

disadvantages include the reliance on slip rings and a complex protective scheme. In this study, a single DFIG symbolizes a set of wind turbines. This methodology has been employed in numerous research. [8] shows that simulations of bulk system dynamics using a single machine equivalent is adequate for most planning studies.

3. Modelling of Wind Turbines System

3.1. Wind Turbine

The generated power P_m of a wind turbine is defined as [9]:

$$P_m = \frac{1}{2}\rho R^2 C_p(\lambda,\beta)V^3 \quad (1)$$

The tip speed ratio λ is defined as:

$$\lambda = \frac{R\varpi_m}{V} \quad (2)$$

The coefficient for power conversion is:

$$C_{\mathrm{p}}(\lambda,\beta) = c_l\left(\frac{c_2}{\Lambda} - c_3\beta - c_4\beta^{c_5} - c_6\right)e^{-\frac{c_7}{\Lambda}} \quad (3)$$

$$\frac{1}{\Lambda} = \frac{1}{\lambda+0.08\beta} - \frac{0.035}{1+\beta^3} \quad (4)$$

Based on (1) and (2), the torque generated by the turbine can be calculated as:

$$T_m = \frac{P_m}{\varpi_m} = \frac{1}{2}\rho\pi R^3 \frac{\mathrm{C_p}(\lambda,\beta)}{\lambda}V^2 \quad (5)$$

In relation to every specified wind velocity, Table 2 presents the associated rotor speed, generated power, and turbine torque data.

Table 2. Rotor speed, mechanical power data

Wind (m/s)	7	8	9	10	11	12
w_m (p.u.)	0.8	0.88	0.97	1.07	1.18	1.2
P_m (p.u.)	0.24	0.31	0.39	0.49	0.64	0.84
T_m (p.u.)	0.3	0.35	0.4	0.46	0.54	0.7

3.2. Mechanical Drive Train

In the analysis of the interrelationship between the drive train of DFIG and the electrical infrastructure, it is noted that low-frequency elements are predominant in shaft vibrations. Consequently, the two-mass model approach may be employed to formulate the equations governing the dynamics of the mechanical drive train [9]:

$$\frac{d}{dt}\begin{bmatrix} w_t \\ w_r \\ T_g \end{bmatrix} = \begin{bmatrix} \frac{-D_t - D_{tg}}{2H_t} & \frac{D_{tg}}{2H_t} & \frac{-1}{2H_t} \\ \frac{D_{tg}}{2H_g} & \frac{-D_t - D_{tg}}{2H_g} & \frac{1}{2H_g} \\ K_{tg}w_e & -K_{tg}w_e & 0 \end{bmatrix}\begin{bmatrix} w_t \\ w_r \\ T_g \end{bmatrix} + \begin{bmatrix} \frac{1}{2H_t} & 0 & 0 \\ 0 & \frac{1}{2H_g} & 0 \\ 0 & 0 & 1 \end{bmatrix}\begin{bmatrix} T_m \\ T_e \\ 0 \end{bmatrix} \quad (6)$$

Parameters of shaft system are given in Table 3.

Table 3. Drive train data

H_t	4.32 sec
H_g	0.685 sec
D_t	0
D_{tg}	1.5 p.u.
K_{tg}	1.11

3.3. Induction Generator Model

Lower-order models (e.g., 2nd or 4th-order) are useful for fast simulations or where stator transients are negligible, but they systematically miss the coupled electromagnetic modes, leading to potential misprediction of damping, stability margins, and transient currents. The sixth-order model is a compromise between fidelity and complexity: it is small enough for system/transient studies yet large enough to retain critical dynamics that lower-order reductions eliminate. Herein, a sixth-order model is employed to characterize the dynamic behaviors of DFIG [12].

The detailed model is expressed as:

$$\dot{X}_g = AX_g + BU \quad (7)$$

where:

$$X_g = \left[i_{qs} i_{ds} i_{0s} i_{qr} i_{dr} i_{0r}\right]^T$$

$$U = \left[v_{qs} v_{ds} v_{0s} v_{qr} v_{dr} v_{0r}\right]^T$$

$$B = \omega_b \begin{bmatrix} X_s & 0 & 0 & X_m & 0 & 0 \\ 0 & X_s & 0 & 0 & X_m & 0 \\ 0 & 0 & X_{ls} & 0 & 0 & 0 \\ X_m & 0 & 0 & X_r & 0 & 0 \\ 0 & X_m & 0 & 0 & X_r & 0 \\ 0 & 0 & 0 & 0 & 0 & X_{lr} \end{bmatrix}^{-1}$$

$$A = -B\begin{bmatrix} R_s & \frac{\omega_s}{\omega_b}X_s & 0 & 0 & \frac{\omega_s}{\omega_b}X_m & 0 \\ -\frac{\omega_s}{\omega_b}X_s & R_s & 0 & -\frac{\omega_s}{\omega_b}X_m & 0 & 0 \\ 0 & 0 & R_s & 0 & 0 & 0 \\ 0 & \frac{\omega_s-\omega_r}{\omega_b}X_m & 0 & R_r & \frac{\omega_s-\omega_r}{\omega_b}X_r & 0 \\ \frac{\omega_r-\omega_s}{\omega_b}X_m & 0 & 0 & \frac{\omega_r-\omega_s}{\omega_b}X_r & R_r & 0 \\ 0 & 0 & 0 & 0 & 0 & R_r \end{bmatrix}$$

Considering that we are analyzing a balanced three-phase system, the zero-sequence specified in (7) can be excluded.

Table 4. DFIG data

Nomial power	1.5 MW
Nominal voltage	575 V
R_s	0.023 p.u.
X_{Ls}	0.18 p.u.
X_m	2.9 p.u.
R_r	0.016 p.u.
X_{Lr}	0.16 p.u.
X_{tg}	0.3 p.u.
DC-link voltage	1200 V
DC-link capacitor	10000 μF

3.4. Power Network

The RLC circuit, represented as the studied system, can be formulated in the following:

$$R_L i_L + L\frac{di_L}{dt} + v_c = v_s - E_{sys} \tag{8}$$

Note that i_L is the current of transmission line, R_L represents transmission line reactance, v_c is the capacitor voltage, v_s is the voltage of generator, E_{sys} is the voltage of system bus.

The d-q frame is frequently employed in the modeling of induction machines [6]. Within this rotating frame, the behavior of the system is characterized as:

$$\frac{\mathrm{d}}{\mathrm{dt}}\begin{bmatrix} i_{qL} \\ i_{dL} \\ v_{cq} \\ v_{cd} \end{bmatrix} = \begin{bmatrix} \frac{-R_L}{X_L} & -\omega_e & \frac{-1}{X_L} & 0 \\ \omega_e & \frac{-R_L}{X_L} & 0 & \frac{-1}{X_L} \\ X_C & 0 & 0 & -\omega_e \\ 0 & X_C & \omega_e & 0 \end{bmatrix}\begin{bmatrix} i_{qL} \\ i_{dL} \\ v_{cq} \\ v_{cd} \end{bmatrix} + \begin{bmatrix} \omega_b & 0 & 0 & 0 \\ 0 & \omega_b & 0 & 0 \\ 0 & 0 & 1 & 0 \\ 0 & 0 & 0 & 1 \end{bmatrix}\begin{bmatrix} \frac{v_{qs}-E_{sysq}}{X_L} \\ \frac{v_{ds}-E_{sysd}}{X_L} \\ 0 \\ 0 \end{bmatrix} \tag{9}$$

where E_{sysd}, E_{sysq} denote voltages of the system bus, and X_C represents the reactance of the series capacitor.

3.5. DC Link

In this paper, the behavior of the DC link connecting the rotor side converter (RSC) and the grid side converter (GSC) is characterized through the application of a first-order differential equation [7].

$$\begin{aligned} C_{DC}V_{DC}\frac{dV_{DC}}{dt} &= P_r - P_g \\ P_r &= 0.5\left(v_{qr}i_{qr} + v_{dr}i_{dr}\right) \\ P_g &= 0.5\left(v_{qg}i_{qg} + v_{dg}i_{dg}\right) \end{aligned} \tag{10}$$

where the parameters P_r and P_g denote the active power associated with the RSC and GSC, respectively.

3.6. Converter Control System

The circuit of DFIG consists of a wound rotor induction generator wherein both the stator and rotor are directly linked to the electrical grid via back-to-back converters, correspondingly. This paper encompasses the modeling of both RSC and GSC controls. Two vector control methodologies within the d-q frames are implemented for the GSC and RSC of DFIG wind turbine systems.

The RSC control system consists of an internal loop dedicated to current regulation and an external loop focused on power management, while the GSC control system features an internal loop for current and an external loop for voltage regulation. The objective of the control system is to maintain a constant DC-link voltage and to manage the grid's reactive power to achieve a value of zero. The configurations of the RSC, GSC control system are illustrated in Fig. 2 and Fig. 3, respectively.

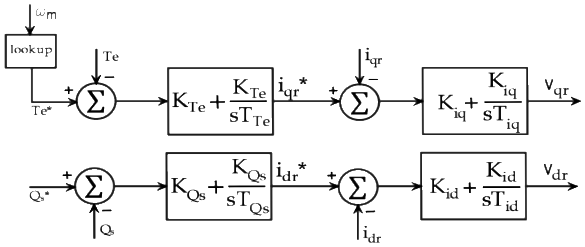

Fig. 2. Block diagram RSC control system

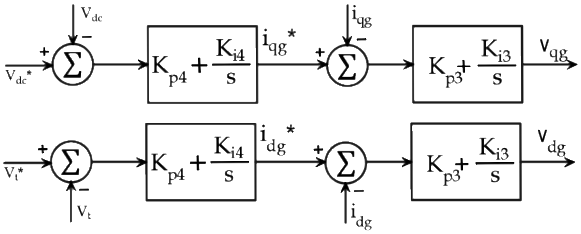

Fig. 3. Block diagram of GSC control system

The reference torque value T_e, which is associated with the wind velocity, is detailed in Table 2. The reference reactive power Q_s is established as zero (indicating a unity power factor). Data pertaining to the converter controller is outlined in [7, 10].

4. Eigenvalues Calculation

Eigenvalue analysis represents a fast and precise approach derived from linear theory. To evaluate the SSR characteristics utilizing the eigenvalue analysis technique, it is essential to formulate a comprehensive mathematical model for every system component. Subsequently, the linear state-space representation is derived by linearizing the system around stable operating conditions.

$$\dot{X} = AX \tag{11}$$

where X represents the state variables of the system, and A denotes the system's state matrix.

The related eigenvalue equation can be calculated as follows:

$$|\lambda \boldsymbol{I} - \boldsymbol{A}| = 0 \tag{12}$$

where $\boldsymbol{I}$ is identity matrix. $\boldsymbol{\lambda}$ is the eigenvalues of matrix $\boldsymbol{A}$, and it can be expressed as $\lambda_i = \sigma_i \pm j\omega_i$.

In Section 3, the comprehensive mathematical representation of the studied system (which consists of the wind turbine, series-compensated transmission line, DFIG, and its controller) is articulated as algebraic equations.

By linearizing the system utilizing state space matrices, the eigenvalues can provide insights into the SSR analysis. MATLAB is a powerful software that provides integrated modules for developing a linearized state-space model and conducting eigenvalue analysis.

The analysis of eigenvalues based on the state-space formulation of the system can efficiently determine the frequency and damping coefficients for all oscillations. The real component of the eigenvalues signifies stability, while the absolute value provides information on damping. The imaginary component reflects the oscillation frequency. For a system to be stable, it is imperative that all eigenvalues are negative.

As inllustrated in Fig. 4, the procedure for calculating system eigenvalues can be outlined in the following manner:

- Input parameters of power network, DFIG, series compensation and wind velocity;

- Determine initial values of power network;

- Calculate initial values of X_g in (7) [11];

- Determine the system state space matrices;

- Calculate the eigenvalues.

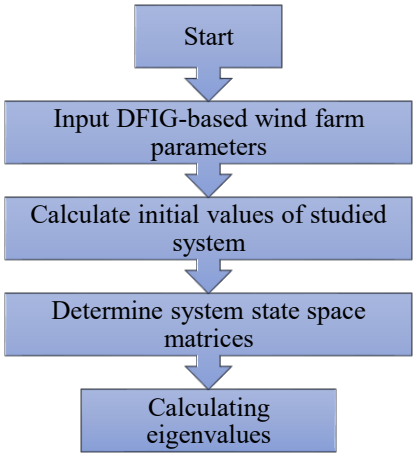

Fig. 4. Calculating eigenvalues flowchart

$$\begin{aligned} i_{dr} &= \left(\frac{\omega_b R_z}{\omega_e X_m} + \frac{X_s v_{ds}}{X_m v_{qs}}\right)_{qG} + \\ &+ \left(\frac{Q_{gvf} X_s}{X_m v_{qr}} - \frac{\omega_b v_{qs}}{\omega_e X_m} - \frac{\omega_b R_s}{\omega_e X_m} i_{ql} - \frac{X_s}{X_m} i_{dq}\right) \\ &= a_I i_{qg} + b_I \end{aligned}$$

$$\begin{aligned} i_{qr} &= \left(\frac{X_s}{X_m} - \frac{\omega_b R_s v_{ds}}{\omega_e X_m v_{qs}}\right) i_{qg} + \\ &+ \left(\frac{\omega_b v_{ds}}{\omega_e X_m} - \frac{X_s}{X_m} i_{ql} + \frac{\omega_b R_s}{\omega_e X_m} i_{dq} - \frac{Q_{gref} \omega_b X_s}{\omega_e X_m v_{qs}}\right) \\ &= a_2 i_{qg} + b_2 \end{aligned} \tag{13}$$

$$\begin{aligned} v_{qr} &= \left(\frac{(\omega_e - \omega_r) X_{mi} v_{db}}{\omega_b v_{qs}} - a_2 R_r - \frac{(\omega_e - \omega_r) X_r a_I}{\omega_b}\right) i_{qg} + \\ &+ \frac{(\omega_e - \omega_r) Q_{gmf} X_B}{\omega_b v_{qs}} - \frac{(\omega_e - \omega_r) X_m}{\omega_b} i_{dl} - \\ &- b_2 R_r - \frac{(\omega_e - \omega_r) X_r b_1}{\omega_b} = a_3 i_{qg} + b_3 \end{aligned}$$

$$\begin{aligned} v_{dr} &= \left(\frac{(\omega_e - \omega_r) X_r a_2}{\omega_b} - a_r R_r - \frac{(\omega_e - \omega_r) X_m}{\omega_b}\right) i_{qB} + \\ &+ \left(\frac{(\omega_e - \omega_r) X_r b_2}{\omega_b} - \frac{(\omega_e - \omega_r) X_m}{\omega_b} i_{ql} - b_r R_r\right) \\ &= a_f i_{qg} + b_4 \end{aligned}$$

$$a_5 i_{qg}^2 + b_5 i_{qg} + c_5 = 0$$

$$a_5 = a_2 a_3 + a_1 a_4$$

$$b_5 = -v_{qs} - v_{ds}^2 / v_{qs} + a_3 b_2 + a_2 b_3 + a_4 b_1 + a_1 b_4$$

$$c_5 = -Q_{gref} / v_{qs} + b_2 b_3 + b_1 b_4$$

$$i_{qs} = -(i_{ql} - i_{qg})$$

$$i_{ds} = -(i_{dl} - i_{qg}{}^{v}{}_{ds} / v_{qs} - Q_{gref} / v_{qs})$$

5. Simulation Results

The system under investigation has been developed using MATLAB as shown in Fig. 5. Time domain simulation is performed with several cases including different wind speeds and compensation levels for SSR analysis. At 0.5s, the three-phase breaker on the non-compensated line is tripped.

It is well-known that the series compensation level k equal X_C/X_L of transmission lines affects the electrical damping of SSR oscillations. X_C and X_L are the transmission lines capacitive reactance and inductive reactance, respectively.

5.1. Influence of Wind Velocity

Considering the standard wind velocities ranging from 7 m/s to 11 m/s, along with a series compensation of 40%, the computed eigenvalues corresponding to various wind speeds are presented in Table 5 and Table 6.

Table 5. Eigenvalues for wind speed 7m/s and compensation level 40%

Eigenvalue	Frequency (Hz)	Type
-1793.5 ± j890.57	40.7	Super syn.
-18.56 ± j547.83	36.4	Super syn.
5.02 ± j211.09	32.9	SSR
-57.914 ± j78.61		
-4.5026 ± j7.55		
3.42 ± j4.29		Torsional
-2.45 ± j0.38		
-0.38 ± j1.14		
-8.08		
0.14		
0		
0		
-48.17		
-37.17		

In Table 6, the real components corresponding to wind velocities from 7 m/s to 9 m/s exceed zero, indicating that these scenarios exhibit instability.

Table 6. Eigenvalues for different wind speed

V (m/s)	Eigenvalues	Type	Frequency (Hz)
7	**5 ± j211.1**	**SSR**	33.6
8	**2.6 ± j209**	**SSR**	33.2
9	**0.4 ± j207**	**SSR**	32.9
10	-1.4 ± j206.6		
11	-3.0 ± j205.9		

The primary mode exhibits a frequency of approximately 33.6 Hz at a wind velocity of 7 m/s, 33.2 Hz at 8 m/s, and 32.9 Hz at a wind speed of 9 m/s.

Since the frequency of electro-mechanical mode is a sub-synchronous counterpart of the turbine, it is significantly influenced by variations in wind speed. Table 5 confirms that witxh an increase in wind speed, the imaginary component exhibits a reduction.

To ascertain the credibility of the eigenvalue analysis technique, a time domain simulation approach was employed to evaluate the cases. Fig. 6 illustrates the dynamic behavior of the electromagnetic power of DFIG. In the case of 10 m/s, it indicates that the system achieves convergence without exhibiting instability.

Furthermore, in comparison to a wind velocity of 11 m/s, the power P_e demonstrates a more rapid convergence. This suggests that the system possesses an enhanced damping characteristic. Meanwhile, for the wind speed of 7 m/s, 8 m/s, and 9 m/s, Fig. 6 shows that the system diverges exhibiting instability after the series capacitor is put into operation, thereby causing the amplitude of the oscillation (P_e).

The outcomes of the simulation are in alignment with the eigenvalue assessment. It can be inferred that high wind speeds do not result in significant harm, whereas light wind speeds induce instability within the studied system.

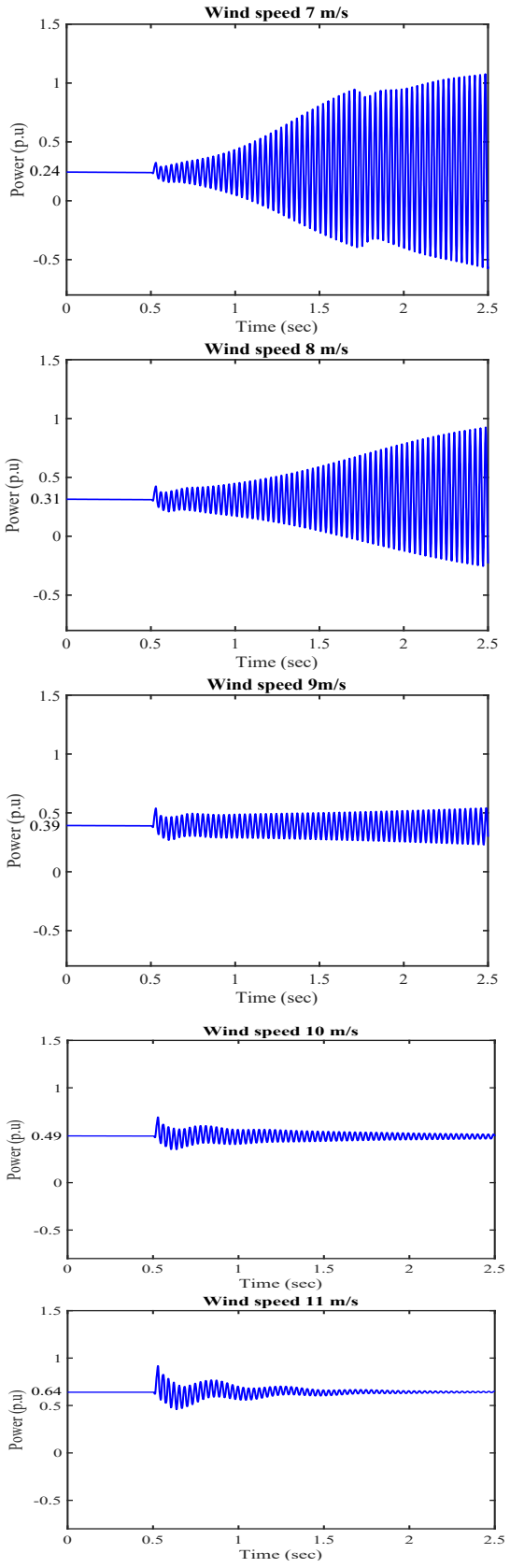

Fig. 6. Electromagnetic power of DFIG for various wind speeds (k = 40%)

5.2. Influence of Series Compensation

The method of eigenvalue analysis was again employed to determine the eigenvalues of the system under varying k, with a wind speed of 10 m/s. The calculated eigenvalues are presented in Table 7.

Table 7. Eigenvalue for different compensation level

Compensation	Eigenvalues	Type	Frequency (Hz)
20%	-3.7 ± j256		40.7
30%	-2.5 ± j229		36.4
40%	-1.4 ± j206.6		32.9
50%	**0.2 ± j182**	**SSR**	28.9
60%	**0.9 ± j170**	**SSR**	27.1

It is evident from Table 7 that the eigenvalues vary with different levels of compensation. When compensation level k is minimal, the real component of the eigenvalue is negative, indicating system stability. As k increases, this effectively reduces the electrical length of the transmission lines, thereby its overall reactance is reduced.

When k exceeds 0.4, the real component of the eigenvalue turns positive, signifying the emergence of low frequency oscillations within the system, with the associated frequencies being 28.9 Hz and 27.1 Hz, respectively.

From Fig. 7, the electrical output of the generator exhibits significant fluctuations, with the amplitude progressively escalating over time at compensation levels of 50% and 60%. This result confirms that the system has lost stability and is experiencing SSR.

It can be concluded that minimal k will not cause much damage while high k may induce instability within the system.

6. Conclusion

In this study, an eigenvalue examination of a wind farm utilizing DFIG linked to a series-compensated transmission line was performed. The findings were utilized to evaluate SSR stability of the system. The analytical results are corroborated through simulations conducted in MATLAB. Two factors that influence the SSR within the system are analyzed. We find that high compensation level (over 50%) causes SSR to occur; light wind speed increased the amplitude of SSR when it occurred (<9 m/s).

These results are important to consider when new wind farm is built to prevent SSR to occur. Hence, investigation of strategies that can damp SSR such as modifying control system parameters, installing supplementary damping controllers, using E-STATCOM or sub-synchronous frequency relay will be our future work.

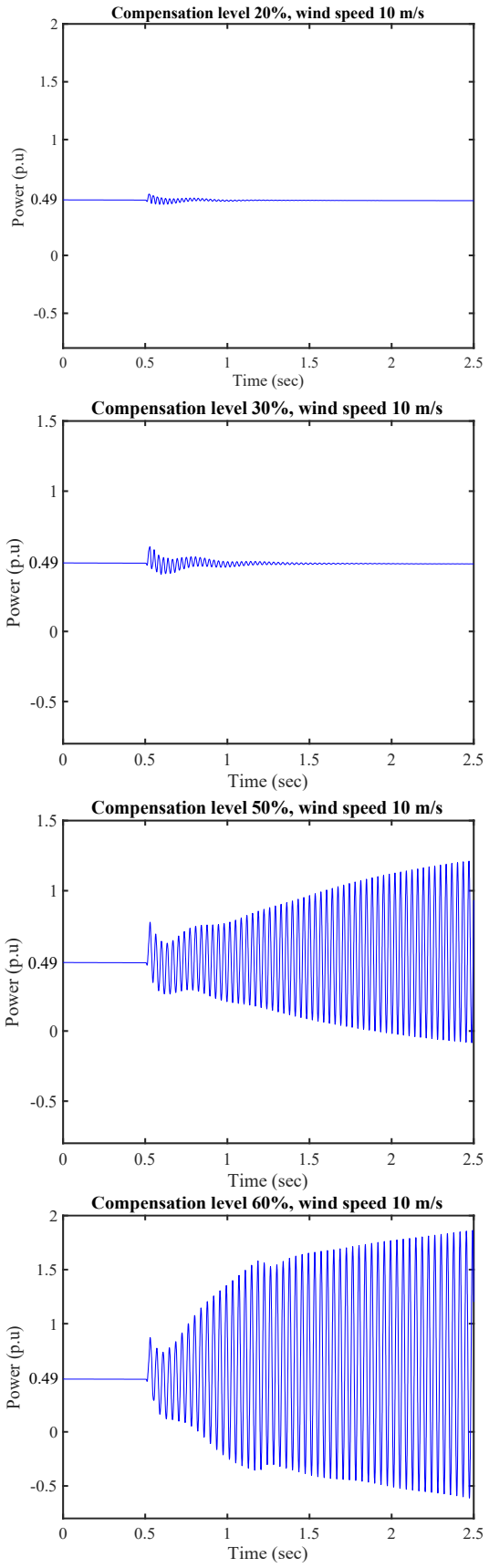

Fig. 7. Simulation results for wind speed 10 m/s and different compensation level

References

[1] L. Wang, X. Xie, Q. Jiang, H. Liu, Y. Li, and H. Liu, Investigation of SSR in practical DFIG-base wind farms connected to series-compensated power system, IEEE Transactions on Power Systems, vol. 30, iss. 5, pp. 2772–2779, Sep. 2015. https://doi.org/10.1109/TPWRS.2014.2365197

[2] X. Dong, X. Tian, Y. Zhang, and J. Song, Practical SSR incidence and influencing factor analysis of DFIG-based series-compensated transmission system in Guyuan Farms, High Voltage Engineering, vol. 43. iss. 1, pp. 327–334, 2017.

[3] A. K. Jindal, Sub-Synchronous interactions with wind farms connected near series compensated AC lines, in Proceedings of 9th International Workshop on Large Scale Integration of Wind Power Systems, Quebec City, Canada, 2010, pp. 559–564.

[4] G. D. Irwin, A. K. Jindal, and A. L. Isaacs, Sub-synchronous control interactions between type 3 wind turbines and series compensated AC transmission systems, in Proceedings of the 2011 IEEE Power and Energy Society General Meeting, Detroit, MI, USA, Jul. 2011. https://doi.org/10.1109/PES.2011.6039426

[5] L. Fan, C. Zhu, Z. Miao, and M. Hu, Modal analysis of DFIG-based wind farm interfaced with a series compensated network, IEEE Transactions on Energy Conversion, vol. 26, iss. 4, Dec. 2011, pp. 1010–1020. https://doi.org/10.1109/TEC.2011.2160995

[6] A. K. Abdulabbas, S. M. Salih, and M. A. Alawan, The analysis of sub-synchronous resonance in a wind farm for a doubly-fed induction generator using modern analytical method, Iraqi Journal for Electrical and Electronic Engineering, vol. 20, no. 1, Mar. 2024. https://doi.org/10.37917/ijeee.20.1.24

[7] Nicholas W. Miller, William W. Price, and J. J. Sanchez-Gasca, Dynamic Modeling of GE 1.5 and 3.6 Wind Turbine-Generators, in 2003 IEEE Power Engineering Society General Meeting, Toronto, ON, Canada, 2003, pp. 1977–1983.

[8] B. Badrzadeh, M. Sahni, D. Muthumuni, Y. Zhou, and A. Gole, Sub synchronous interaction in wind power plants - Part I: Study tools and techniques, in Proceedings of the IEEE PES General Meeting, San Diego, California, USA, 2012. https://doi.org/10.1109/PESMG.2013.6672545

[9] S. M. Muyeen, M. H. Ali, R. Takahashi, T. Murata, J. Tamura, and Y. Tomaki, Transient stability analysis of wind generator system with the consideration of multi-mass shaft model, in 2005 International Conference on Power Electronics and Drive Systems, Kuala Lumpur, Malaysia, 2005, pp. 511–516.

[10] F. Mei and B. Pal, Modal analysis of grid-connected doubly-fed induction generators, IEEE Transactions on Energy Conversion, vol. 22, no. 3, pp. 728–736, Sep. 2007. https://doi.org/10.1109/TEC.2006.881080

[11] M. Wu and L. Xie, Calculation steady-state operating conditions for DFIG-based wind turbines, IEEE Transactions on Sustainable Energy, vol. 9, iss. 1, pp. 293–301, Jan. 2018. https://doi.org/10.1109/TSTE.2017.2731661

[12] B. Lu, S. Li, H. S. Das, Y. Gao, J. Wang, and M. Baggu, Dynamic P-Q capability and abnormal operation analysis of a wind turbine with doubly fed induction generator, IEEE Journal of Emerging and Selected Topics in Power Electronics, vol. 10, iss. 4, Aug. 2022. https://doi.org/10.1109/JESTPE.2021.3133527

Nomenclature

ρ	Air density [kg/m^3]
R	Blade's radius [m]
V	Speed of wind [m/s]
$C_p(\lambda,\beta)$	Efficiency conversion factor
λ	Tip speed
β	Pitch angle
ω_m	Rotor speed of wind turbine
K_{tg}	Shaft stiffness coefficient of drive train
D_{tg}	Damping coefficient between wind turbine and generator
D_t	Damping coefficient of wind turbine
D_g	Damping coefficient of DFIG
H_t	Inertia constants of the wind turbine
H_g	Inertia constants of DFIG
ω_t	Angular speed of wind turbine
ω_r	Angular speed of DFIG's rotor
T_e	Electromagnetic torque of DFIG
R_s, X_s, X_{ls}	Stator resistance, reactance and leakage reactance
R_r, X_r, X_{lr}	Rotor resistance, reactance and leakage reactance
X_m	Magnetizing reactance
w_b	Base speed
w_s	Synchronous frame frequency
$c_{1,..,}$ c_7	Constants
Subcripts:	
s, r	Stator and rotor side
d, q	Direct and quadrature component of electrical signal in rotating reference frame